

# Journal of Materials Chemistry A

Accepted Manuscript



This is an *Accepted Manuscript*, which has been through the Royal Society of Chemistry peer review process and has been accepted for publication.

*Accepted Manuscripts* are published online shortly after acceptance, before technical editing, formatting and proof reading. Using this free service, authors can make their results available to the community, in citable form, before we publish the edited article. We will replace this *Accepted Manuscript* with the edited and formatted *Advance Article* as soon as it is available.

You can find more information about *Accepted Manuscripts* in the [Information for Authors](#).

Please note that technical editing may introduce minor changes to the text and/or graphics, which may alter content. The journal's standard [Terms & Conditions](#) and the [Ethical guidelines](#) still apply. In no event shall the Royal Society of Chemistry be held responsible for any errors or omissions in this *Accepted Manuscript* or any consequences arising from the use of any information it contains.

## A monolithic and standalone solar-fuel device having comparable efficiency to photosynthesis in nature

Hyo Sang Jeon,<sup>a,b</sup> Jai Hyun Koh,<sup>a</sup> Se Jin Park,<sup>a</sup> Michael Shincheon Jee,<sup>a</sup> Doo-Hyun Ko,<sup>c</sup> Yun Jeong Hwang<sup>a,b</sup> and Byoung Koun Min<sup>a,b,d</sup>

Received (in XXX, XXX) Xth XXXXXXXXX 20XX, Accepted Xth XXXXXXXXX 20XX  
DOI: 10.1039/b000000x

Artificial photosynthesis inspired from nature has attracted academic and industrial attention due to a need for developing sustainable energy sources. In this study, we demonstrate a highly efficient solar energy to fuel conversion device using CO<sub>2</sub> and water as feedstock. We developed a thin film photovoltaic technology for the light absorbing component using a low cost, solution based Cu(In<sub>x</sub>Ga<sub>1-x</sub>)(S<sub>y</sub>Se<sub>1-y</sub>)<sub>2</sub> (CIGS) module fabrication method to provide high enough potential for the conversion reactions. Our solar-fuel device adapted cobalt oxide (Co<sub>3</sub>O<sub>4</sub>) nanoparticle thin film deposited with a low temperature coating method as the water oxidation catalyst and nanostructured gold film as the CO<sub>2</sub> reduction to CO generation catalyst. We demonstrated that the integrated monolithic device operated by the energy only from sunlight in an absence of any external energy input in which each individual components showed following abilities: sunlight-to-electricity conversion efficiency of 8.58% for the CIGS photovoltaic module photoelectrode, overpotential reduction of water oxidation by the Co<sub>3</sub>O<sub>4</sub> catalyst film of up to ~360 mV at 5 mA/cm<sup>2</sup> overpotential for water oxidation, and Faradaic efficiency of over 90% by the nanostructured Au catalyst for CO<sub>2</sub> reduction to CO. Remarkably, this is the first demonstration of a monolithic and standalone solar-fuel device whose solar-to-fuel conversion efficiency from CO<sub>2</sub> and H<sub>2</sub>O is 4.23%, which is comparable to that of photosynthesis in nature.

### 1. Introduction

World energy production still heavily depends on the traditional fossil fuels which are to blame for global climate changes due to greenhouse gas emissions, and uneven distribution of the fossil fuels in the world even worsens international conflicts.<sup>1,2</sup> To resolve these issues, tremendous efforts have been put in developing sustainable energy resources to replace fossil fuels. Among various energy production methods, fuel production from solar energy is one of the most promising approaches because the solar energy is more than abundant to supply the increasing world energy consumption and it can be stored as fuels.<sup>3</sup> Such conversion system is often called “artificial photosynthesis”, mimicking the photosynthesis in plants to produce hydrocarbon fuels from sunlight, CO<sub>2</sub>, and water; where the products are deemed “solar-fuels”.<sup>4</sup> A variety of attempts to produce solar fuels artificially have been suggested using multi-functional photocatalysts<sup>4-6</sup> or photoelectrochemical devices.<sup>7-10</sup> However, none of solar-fuel generating systems showed promising efficiencies, even performing poorer than photosynthesis in nature. The efficiency of photosynthesis in nature is very diverse depending on a specific system. For example, C3 plants producing three-carbon sugar, which include algae, reach 3.5% efficiency under optimal conditions during their growing season; and C4 plants producing four-carbon compound, which include

angiosperms, can have up to 4.3%.<sup>11</sup> However, photosynthesis efficiencies of common plant leaves are known to be lower than 1% due to inconsistent insolation and limited CO<sub>2</sub> concentration in the atmosphere.<sup>11-13</sup> Therefore, it may be the first challenge to make an artificial solar-fuel device whose efficiency is comparable to those in nature.

To design an efficient solar-fuel device, it may be reasonable to revisit solar-water splitting systems because tremendous researches have been done over 40 years since its first demonstration by Fujishima and Honda.<sup>14</sup> Several representative results of photo-water splitting systems are summarized in Table S1, ESI†. Rigid material requirements for solar-water splitting make it unachievable to reach high solar-to-hydrogen (STH) conversion efficiencies solely with metal oxide photocatalytic materials in spite of the beneficial aspects of their low cost. On the other hand, solar-water splitting systems with photovoltaic (PV) technology incorporated within photoelectrodes have revealed relatively high efficiencies. For example, when a triple junction amorphous Si PV technology was incorporated within catalytic electrodes, 4.7% of STH efficiency was achieved (see Fig. 1a).<sup>15</sup> More surprisingly, in a case with III-V compound, PV technology incorporated into a tandem structure with p-type GaInP<sub>2</sub> photocatalytic material already achieved over 12% STH efficiency 15 years prior, although cost as well as stability issues still remain (see Fig. 1b).<sup>16</sup> When PV technology was incorporated, the operating current and

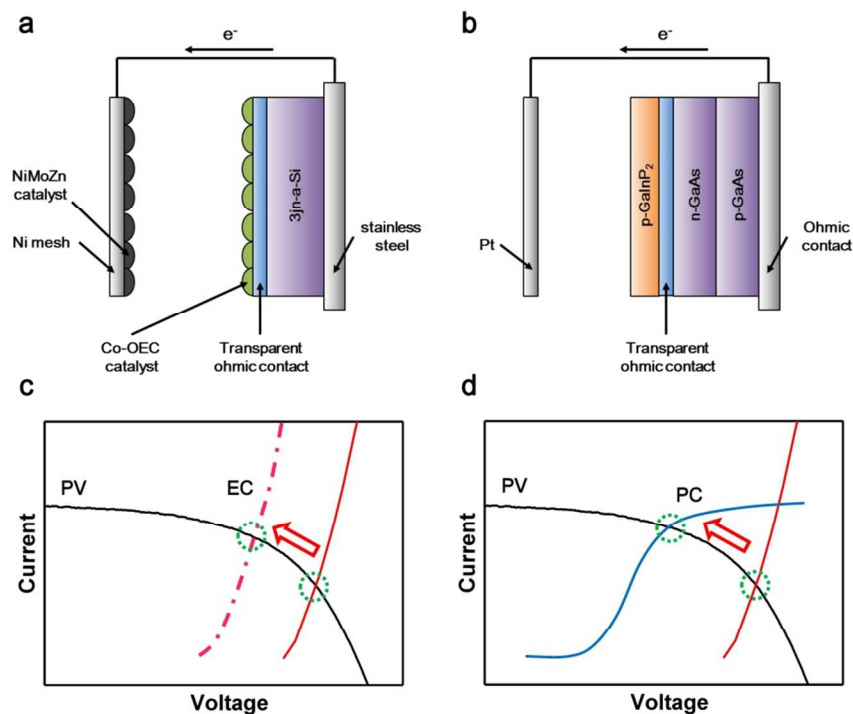


**Fig. 1** Designs for solar-fuel devices. (a) Schematic diagram of a representative PEC water splitting cell developed by Nocera's group with Co-OEC | 3j(n-a-Si) | NiMoZn cell configuration. (adapted from ref. 14) (b) Schematic diagram of a representative PEC water splitting cell developed by Turner's group with GaAs PV within p-GaInP<sub>2</sub> photo-cathode. (adapted from ref. 15) Schematic diagrams to illustrate the enhancement operating current of a solar-fuel device by incorporating (c) electrocatalysts (EC) of low overpotentials, or (d) photocatalysts (PC).

consequential STH efficiency are determined by the intersecting point between the I-V curves of the PV cell and catalytic electrodes.<sup>17</sup> There are two approaches that can be applied to enhance the STH efficiency. The operating point can be shifted to a higher current (short circuit current,  $I_{sc}$ , is the maximum) and lower voltage (minimizing input-energy) by i) reducing overpotentials for overall water-splitting on either anode or cathode with highly efficient electrocatalyst (EC) (see Fig. 1c)<sup>18</sup> or ii) combining photocatalyst (PC) materials to (photo)anode or (photo)cathode to utilize the charge separation at the photocatalyst/electrolyte junction (see Fig. 1d)<sup>19</sup>. Notably, the use of PC is preferable over EC since water splitting at zero bias (in an absence of PV) is theoretically possible,<sup>20</sup> which triggers tremendous efforts on development of semiconductor PC materials, despite the technical difficulty with tandem integration. The structure of Fig 1b is limited to a system in which band gap of the semiconductor in PV cell is smaller than that of the PC materials for the efficient light absorption since light passes through the PC layer first, although a wide band gap material is more favorable to obtain a large open circuit potential in the PV part. Therefore, structures of the efficient solar-fuel device have to deliberately designed to be applicable for both systems (PV cell integrated with EC or PC) with a variety of material choices. After closely reviewing the representative solar-water splitting systems mentioned above, we found that the PV part (p-n junction of semiconductors) and photocatalyst or electrocatalyst films ohmically connected in the electrolyte by a transparent conducting film (e.g. ITO layer) were in common as described schematically in Fig. 2a. If the substrate (e.g. glass) has

conductive properties on both sides, the substrate itself can be used as a ohmic contact between PV and photocatalytic or electrocatalytic film instead of the thin layer of a conducting material, deriving an idea where PV part is placed out of the electrolyte, while still maintaining ohmic connection with photocatalytic or electrocatalytic film through the conductive substrate (e.g. glass with ITO layer on both sides, see Fig.2b and Fig. 2c). This configuration has a merit in terms of durability of the PV part because it is not directly contact with the electrolyte. In general, semiconductor materials such as silicon and GaAs used in PV are vulnerable in aqueous electrolyte environment.<sup>21</sup> In addition, the incident light can now reach the PV and PC films without absorption or scattering loss by the aqueous electrolyte,<sup>22</sup> minimizing the efficiency loss of each integrated component. To test the proposed configuration for solar-fuel devices, in this study, Fig. 2c was proven as a model system that incorporates PV technology with EC. Particularly, we demonstrate a solar-fuel device with parallel series connection of single junction PV cells (i.e. module) using a well-established module fabrication process to supply high enough energy for both water splitting and CO<sub>2</sub> reduction in the device, although there is some photocurrent loss due to reduction of active area of absorber film compared to vertical series connection of single cells. In our long journey to realize a highly efficient, low cost, outstandingly stable monolithic and standalone solar-fuel device, we demonstrate a first model of solar-fuel device which has comparable solar-to-fuel conversion efficiency to that of photosynthesis in nature. In this device, Cu(In<sub>x</sub>Ga<sub>1-x</sub>)(S<sub>y</sub>Se<sub>1-y</sub>)<sub>2</sub> (CIGS) thin film solar cell technology was applied in the PV part.

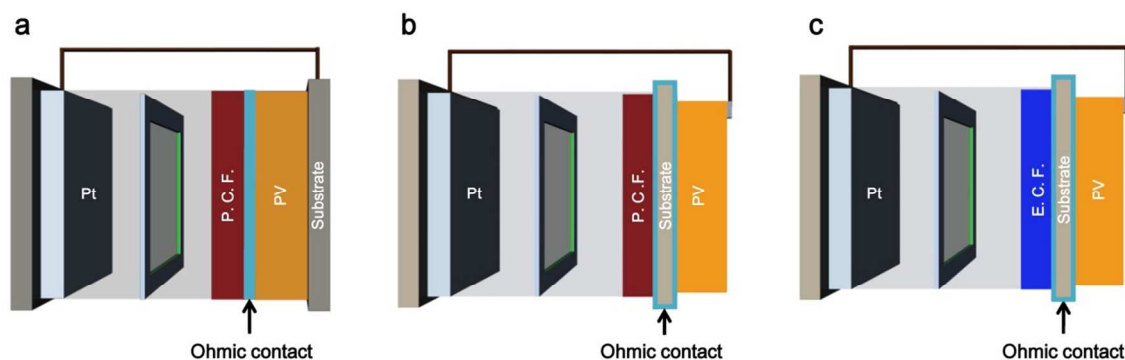


**Fig. 2** (a) Solar-fuel device with photocatalytic film (P.C.F.) and internal PV. (b) Solar-fuel device with photocatalytic film (P.C.F.) and external PV. (c) Solar-fuel device with electrocatalytic film (E.C.F.) and external PV.

Unlike the commercialized CIGS thin film solar cell technology (a vacuum based method) we adapted a low cost solution based method for fabricating the CIGS absorber film which is expected to be more beneficial in terms of cost, throughput, and scale-up.<sup>23</sup> Since a single junction CIGS cell cannot provide a sufficient photovoltage for thermodynamic energy to compensate for the water splitting/ $\text{CO}_2$  reduction overpotential, CIGS module was fabricated on a single glass substrate. On reverse side of this PV module, electrocatalytic film ( $\text{Co}_3\text{O}_4$ ) for water oxidation was monolithically prepared based on a low temperature coating method in order to not damage the performance of the pre-made PV part. Nanostructured gold was applied as the electrocatalyst for selective reduction of  $\text{CO}_2$  to CO, since it requires relatively low overpotential with a high Faradaic efficiency for  $\text{CO}_2$  reduction in aqueous media. Each component was successfully incorporated into a standalone solar-fuel device, with only ~5% coupling efficiency loss. We demonstrate that the actual model device has 4.23% solar to CO chemical conversion efficiency, which is comparable to or even higher than the conversion efficiency of photosynthesis in nature.

## 2. Experimental

### 2.1. CIGS module fabrication

CIGS module was fabricated on a patterned molybdenum (Mo) layer. The Mo layer (~1  $\mu\text{m}$ ) was sputtered on a soda lime glass, and the first pattern, P1 (see Fig. S1, ESI†), was scribed by nanosecond pulsed laser with 532 nm wavelength. The laser beam was incident from the soda lime glass side to avoid any thermal damage of Mo back contact by laser scribing. A solution processed CIGS absorber layer was then spin-coated onto the patterned Mo. A precursor mixture solution was prepared by dissolving appropriate amounts of  $\text{Cu}(\text{NO}_3)_2 \cdot x\text{H}_2\text{O}$  (Aldrich, 1.0 g),  $\text{In}(\text{NO}_3)_3 \cdot x\text{H}_2\text{O}$  (Aldrich, 1.12 g), and  $\text{Ga}(\text{NO}_3)_3 \cdot x\text{H}_2\text{O}$  (Alfa Aesar, 0.41 g) in methanol (10.0 mL), followed by adding a methanol solution (7.0 mL) with polyvinyl acetate (PVA) (Aldrich, 1.0 g). The mixture solution was thoroughly stirred for 30 min prior to spin coating of the precursor solution, and the deposited film was annealed at 300  $^\circ\text{C}$  for 30 min. To obtain the desired thickness of the film (~1.2  $\mu\text{m}$ ), the aforementioned process was repeated about six times (generally ~200 nm thick

film was obtained for each spin coating process). Then, the film was selenized/sulfurized at 470  $^\circ\text{C}$  to form CIGS absorber layer. Later, a 60 nm thick CdS buffer layer was deposited onto the CIGS film by chemical bath deposition (CBD) method, and top contact layer of i-ZnO (50 nm)/Al-doped n-ZnO (500 nm) were deposited by the radio frequency magnetron sputtering. The second (P2) and third (P3) patterns were scribed mechanically before and after deposition of Al-doped n-ZnO, respectively. The whole module area exposed for light illumination was 2.1  $\text{cm}^2$  with 5 single cells having a respective area of 0.42  $\text{cm}^2$ .

### 2.2. Preparation of $\text{Co}_3\text{O}_4$ film

After CIGS module was fabricated, 30 nm of Ti thin film followed by 50 nm of Pt thin film were sputtered on the rear side of the module for the contact of oxidation catalyst particles. Subsequently,  $\text{Co}_3\text{O}_4$  (~50 nm, Aldrich) catalyst film was deposited on the Ti/Pt film by a doctor blade coating method.  $\text{Co}_3\text{O}_4$  catalyst was dispersed in iso-propanol (J. T. Baker) and a Nafion solution (20 wt%, DuPont) was added to prepare a paste. After the  $\text{Co}_3\text{O}_4$  was pasted, the sample was placed on a hotplate at 70  $^\circ\text{C}$  in air.

### 2.3. Preparation of nanostructured Au

Nanostructured Au was prepared by an electrochemical method adapted from ref. 24. The polycrystalline gold foil (99.99%, Dasom RMS) was cleaned in aqua regia, and amorphous Au oxide was fabricated by pulsed anodization. 1.2 V ~ 3.5 V vs. a  $\text{Hg}/\text{Hg}_2\text{SO}_4$  reference electrode (CHI151, CH Instruments, Inc) was applied for 65,000 cycles in aqueous 0.5 M  $\text{H}_2\text{SO}_4$  electrolyte with a potentiostat (Ivium, Iviumtechnology), and a platinum counter electrode was used. The gold oxide was reduced to gold catalysts at -1.0 V vs.  $\text{Ag}/\text{AgCl}$  for 15 min prior to  $\text{CO}_2$  reduction in aqueous 0.5 M  $\text{NaHCO}_3$  solution saturated with  $\text{CO}_2$ .

### 2.4. Electrochemical measurements

All of the electro-catalytic measurements were conducted by using a potentiostat (Ivium, Iviumtechnology) in a two compartment electrochemical cell made of polyether ether ketone (PEEK), and a proton exchange membrane (Nafion<sup>®</sup>, 117) was used to separate anode and cathode sides. 0.5 M  $\text{KHCO}_3$  ( $\geq 99.99\%$ , Aldrich) electrolyte was saturated with  $\text{CO}_2$  whose pH was 7.03 after saturation. A platinum counter electrode and a

Ag/AgCl reference electrode were used in a three-electrode configuration to characterize the catalytic activities of the  $\text{Co}_3\text{O}_4$  nanoparticle film and the nanostructured Au film for water oxidation and  $\text{CO}_2$  reduction, respectively. All potential values were converted in terms of reversible hydrogen electrode (RHE) using  $E$  (vs. RHE) =  $E$  (vs. Ag/AgCl) + 0.197 + 0.059 V  $\times$  pH. Steady-state current density was measured by using chronoamperometry technique with respect to each fixed potential.

### 2.5. Products analysis for $\text{CO}_2$ reduction

The  $\text{CO}_2$  reduction experiments coupled with water oxidation were conducted in both two- and three-electrode configurations. While the three-electrode configuration was performed in a gas-tight two compartment electrochemical cell as described above, the gas products (*i.e.*  $\text{H}_2$  and  $\text{CO}$ ) were quantified by gas chromatography (Younglin 6500 GC) equipped with a pulsed discharge detector (PDD) using ultra high purity (UHP) He (99.9999 %) as the carrier gas. GC was directly connected to the electrochemical cell and the gaseous samples were injected by a six-port valve. Each compartment of the electrochemical cell contained 38 mL of electrolyte and 34 mL of headspace and  $\text{CO}_2$  gas was bubbled through the electrolyte at an average rate of 120 ml/min. The Faradaic efficiencies (F.E.) of  $\text{H}_2$  and  $\text{CO}$  production were calculated from the areas of GC chromatogram as below since both of them are two electron reactions:

$$\text{F.E.}_{\text{H}_2 \text{ or CO}} = V_{\text{H}_2 \text{ or CO}} \times \text{flow rate} \times \frac{2Fp_0}{RT_0 i_{\text{total}}} \quad (1)$$

where  $V_{\text{H}_2 \text{ or CO}}$  are volume concentration of  $\text{H}_2$  or  $\text{CO}$  based on calibration of the GC, flow rate (ml/min) was measured by a universal flow meter (ADM 2000, Agilent Technologies) at the exit of the electrochemical cell.  $i_{\text{total}}$  (mA) is a steady-state current,  $F = 96485 \text{ A}\cdot\text{s}/\text{mol}$ ,  $p_0 = 1.013 \text{ bar}$ ,  $T_0 = 273.15 \text{ K}$ , and  $R = 8.314 \text{ J}\cdot\text{mol}^{-1}\cdot\text{K}^{-1}$ . Formate concentration was analyzed by an ion chromatography (IC, DIONEX IC25A) with a conductivity detector. In order to account for headspace equilibration time, the F.E. of gas products was normalized so that the sum of efficiencies was equaled to 100 %.

In the case of a two-electrode measurement for Fig. 4b, the nanostructured Au film was connected in the cathodic side and the  $\text{Co}_3\text{O}_4$  nanoparticle film was connected in the anodic side without any reference electrode. The products from cathodic compartment were analyzed in a same way as describe above.

### 2.6. Characterization of solar-fuel device

After preparation of all electrodes and acrylic spacer, each component was assembled with epoxy resin as shown in Fig. 4a. The photocurrent was measured by using the two-electrode configuration under AM-1.5G illumination conditions ( $100 \text{ mW}/\text{cm}^2$ ) facing CIGS module to incident light outside of the cell. GC was directly connected to the solar-fuel device and chemical products were quantified following the same procedure as describe above. A solar simulator (ABET, Sun 2000) equipped with a 300 W Xe lamp and air mass (AM) 1.5 filter was used to generate simulated solar light.  $^{13}\text{C}$  isotope experiment was carried out with a gas chromatograph (GC, 6890N network, Agilent Technologies) equipped with a mass-selective detector (MSD, 5973 network, Agilent Technologies).

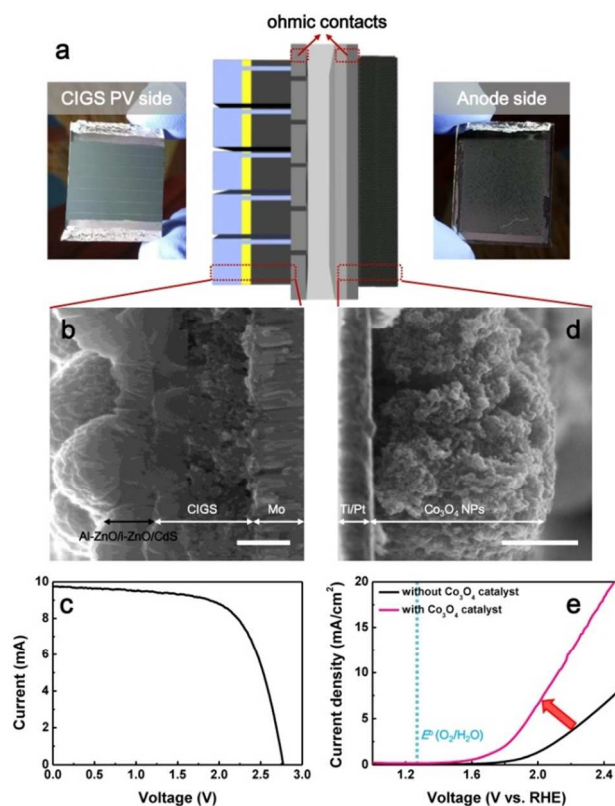


**Fig. 3 Monolithic CIGS module and  $\text{Co}_3\text{O}_4$  anodic catalyst for photoelectrode.** (a) Schematic diagram and photograph of a monolithically stacked photoelectrode with CIGS PV module and  $\text{Co}_3\text{O}_4$  film on each side of the glass substrate. (b) Cross-sectional SEM image of a CIGS PV cell (scale bar is  $1 \mu\text{m}$ ). (c) Typical I-V characteristic of a CIGS module. (d) Cross-sectional SEM image of  $\text{Co}_3\text{O}_4$  film on the glass/Ti/Pt substrate (scale bar is  $1 \mu\text{m}$ ). (e) Typical J-V characteristic of with and without  $\text{Co}_3\text{O}_4$  catalyst films.

### 2.7. Characterizations

The surface morphologies were imaged by field emission gun scanning electron microscopy (FEG-SEM, Inspect F, FEI).

## 3. Results and Discussion

One of the most important components in the solar-fuel device is the photoelectrode that is capable of producing power by absorbing light. Particularly in this study, we employed a photoelectrode that was a combination of PV and electrocatalytic film on a single conducting glass substrate; one side formed the CIGS module for light absorption, the other side made the anode with  $\text{Co}_3\text{O}_4$  nanoparticles catalyst for water oxidation. (see Fig. 3a). Moreover, in order to realize a cost effective fabrication of CIGS film, we adapted a paste coating method which has been developed by our lab.<sup>25,26</sup> To achieve the high single CIGS thin film solar cell voltage, a unit in the module, a selenization process was modified with an addition elemental sulfur (S/Se+S = 40%) to increase the band-gap of the CIGS absorber material. The average open circuit voltage ( $V_{\text{oc}}$ ) of a single solar cell was measured to be 550 mV, and five single cells in parallel achieved a  $V_{\text{oc}}$  of over 2.70 V. The CIGS module was fabricated on a laser-patterned Mo substrate (see Fig. S1, ESI†).

As shown in the cross-sectional SEM image (see Fig. 3b), the CIGS layer with a very low degree of porosity was observed with

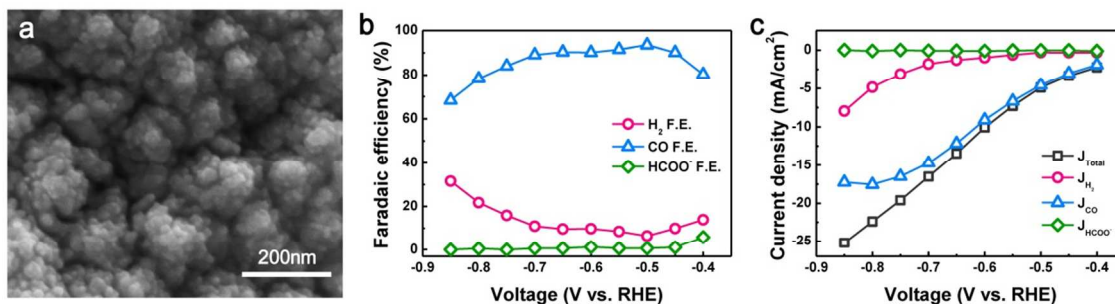


**Fig. 4 Nanostructured Au for cathodic catalyst.** (a) SEM images of nanostructured Au cathodic catalyst. (b) Faradaic efficiency of H<sub>2</sub>, CO, and formate at varying potential on nanostructured Au cathode for CO<sub>2</sub> reduction. (c) Total and partial current densities of H<sub>2</sub>, CO, and formate at varying potential on nanostructured Au cathode for CO<sub>2</sub> reduction.

a conventional Mo/CIGS/CdS/i-ZnO/Al-ZnO structure even with the solution based process. Interestingly, the CIGS layer exhibits two layers with small-sized grains at the interfacial region of the Mo substrate and large-sized grains on the small-sized grains layer (see Fig. S2, ESI†). The formation of two layers was found to be attributable to the difference in the distribution of sulfur and selenium during the selenization process. The current–voltage (*I*–*V*) characteristic of the CIGS module had an efficiency of 8.58% with an open circuit voltage (*V*<sub>oc</sub>), short circuit current (*I*<sub>sc</sub>), and fill factor of 2.77 V, 9.74 mA, and 66.9%, respectively (Fig. 3c), implying that the *V*<sub>oc</sub> of the individual single CIGS cell was successfully maintained in the module configuration.

Next, electrocatalytic film for water oxidation was monolithically integrated with the prepared CIGS module. Catalytic function of an anode side for oxygen evolution is important to achieve a highly efficient reaction because a large overpotential involved with four electron water oxidation process.<sup>27</sup> Particularly, a low temperature coating method to depositing the catalyst at the reverse side is required to protect the pre-made CIGS module on the obverse side. We developed the catalyst film on glass/Ti/Pt substrate with doctor blade coating method by using Co<sub>3</sub>O<sub>4</sub> nanoparticle as the oxygen evolution reaction (OER) catalysts and Nafion solution as the binder material and heat treatment at 70 °C.<sup>28,29</sup> Approximately 2 μm thick film of agglomerated Co<sub>3</sub>O<sub>4</sub> nanoparticles of ~50 nm was observed in the cross-sectional SEM image (see Fig. 3d), which had a porous morphology with high surface area. To investigate OER catalytic performance, linear sweep voltammetry (LSV) was performed in CO<sub>2</sub> saturated 0.5M KHCO<sub>3</sub> electrolyte (see Fig. 3e). Apparent enhancement in water oxidation activity by incorporating Co<sub>3</sub>O<sub>4</sub> catalyst was observed at current response of whole potential region compared to that of the conducting substrate (Ti/Pt thin film). The overpotential corresponding to 5 mA/cm<sup>2</sup> was decreased by 360 mV in the presence of the Co<sub>3</sub>O<sub>4</sub> nanoparticle catalysts (from 2.30 V to 1.94V vs. RHE). Oxygen evolution on the Co<sub>3</sub>O<sub>4</sub> anode was confirmed with the Faradaic efficiency of 97.6 % (±14.3), and slow desorption of oxygen bubbles from the anode surface caused the relatively large standard deviation. Moreover, we could confirm that performance of CIGS module was not damaged even after Co<sub>3</sub>O<sub>4</sub> catalyst deposition (see Fig. S3, ESI†).

Cathode for CO<sub>2</sub> reduction was fabricated by nanostructured gold foil which was synthesized based on the method developed by Chen *et al.*<sup>24</sup> The synthesized nanostructured Au morphology was

characterized by SEM as shown in the Fig. 4a. We could confirm that a surface layer formation with agglomerated tens of nanometer-sized Au particles. Fig. 4b and c show Faradaic efficiencies for H<sub>2</sub>, CO and HCOO<sup>-</sup>, and steady-state current densities of nanostructured Au with respect to potential from -0.39 V to -0.84 V vs. RHE in CO<sub>2</sub> saturated 0.5M KHCO<sub>3</sub> electrolyte. Faradaic efficiency for CO had an optimal potential window from -0.44 V to -0.69 V continuously maintaining around 90 ~ 94% but started to decrease from potentials higher than -0.70 V. Considering the thermodynamic equilibrium potential for CO<sub>2</sub> reduction to CO is -0.10 V vs. RHE, the overpotential at 5 mA/cm<sup>2</sup> was 400 mV. In contrast, Faradaic efficiency of H<sub>2</sub> showed an opposite phenomenon. Observation of the partial current densities for H<sub>2</sub> and CO (see Fig. 4c) show that, under highly biased potential (< -0.7 V vs. RHE), the production rate of H<sub>2</sub> dramatically increase while production rate for CO remain almost constant. This may be a result of mass transfer limitations of CO<sub>2</sub> at the high potential region.<sup>30</sup> In addition, we confirmed the formate ion had < 1% F.E. for most of the potential region with the exception of 5.8% F.E. at 0.39 V vs. RHE.

Photoanode (CIGS PV + Co<sub>3</sub>O<sub>4</sub> OER catalyst) and cathode (nanostructured Au) were then put together to be a monolithic solar-fuel device (see Fig. 5a). Nafion membrane was installed between anode and cathode to separate products from both electrodes and to transfer protons from anode to cathode as well. CO<sub>2</sub> saturated 0.5M KHCO<sub>3</sub> solution was used for both anolyte and catholyte. The acrylic spacer was customized to hold the solution and the spacer and the electrodes were assembled with epoxy resin so that the produced gases can be collected. The device was directly connected to a gas chromatography (GC) in order to determine the device performance on generating products. When a two-electrode experiment was carried out to confirm the CO<sub>2</sub> reduction performance, we could confirm a similar *I*–*V* behavior with the three-electrode test with the nanostructured Au (see Fig. 5b). We could also confirm that the *I*–*V* curve of two-electrode test was divided into three regions. At first region, no chemical reaction occurred due to a non-faradaic process below 2.0 V. The production rate of CO was dramatically increased from 2.0 V to 2.5 V while the production rate for H<sub>2</sub> began to increase from 2.5 V. Thus, a very narrow region for CO generation must be match with CIGS module to get the highly efficient solar to CO production efficiency. When the current was matched to determine the operating point of the prepared CIGS

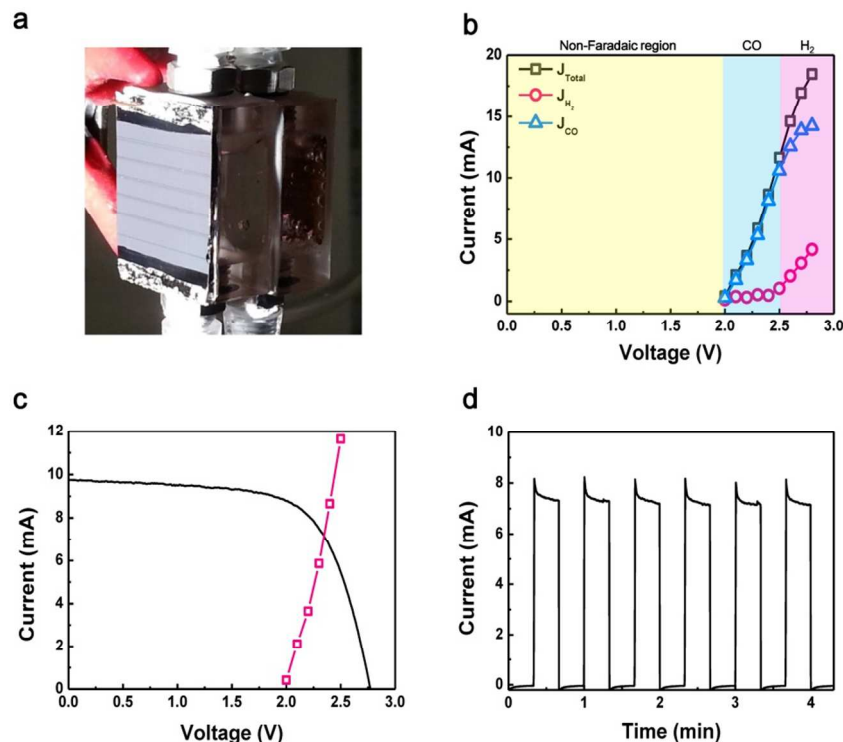


**Fig. 5 Solar-fuel device performance.** (a) Photograph of illuminated solar-fuel device in operation, in which the CIGS module was incorporated at the external side of the PEC cell. (b) Steady-state I-V curves of two-electrode measurement composed of the  $\text{Co}_3\text{O}_4$  nanoparticle film anode and the nanostructured Au cathode showing the 2.0 V of a minimum external potential was required to initiate the overall reactions. (c) I-V characteristics of CIGS module and two-electrode test where the intersection is the operating point for solar-fuel device without any external bias potential. (d) The operating current of the solar-fuel device under the chopped light illumination.

module and  $\text{H}_2\text{O}/\text{CO}_2$  electrolysis, we confirmed that the operating point was the 7.12 mA at 2.34 V (see Fig. 5c).

In order to confirm the performance of the solar-fuel device, the photocurrent was measured as a function of time with no external bias by connecting with external conducting material at the device. As shown in the Fig 5d, a current spike at the moment of illumination and the subsequent decrease to a current was observed. This behavior is attributed to the charging of the double layer and the conversion of reaction adsorbates on the electrode surfaces.<sup>21</sup> After stabilization of photocurrent, we could observe a slight lowering of the photocurrent due to the bubble formation on the EC films. Based on this data, an average photocurrent of about 7.32 mA with 91.2% CO F.E. was directly measured with the actual device, which indeed corresponds to the operating current with the operating voltage of 2.33 V. From this data, solar to fuel conversion efficiency ( $\eta_{\text{STF}}$ ) was calculated by the following equations,<sup>31,32</sup>

$$\eta_{\text{STF}} = \frac{I_{\text{op}} \times \Delta E \times \xi}{P_{\text{in}} \times \text{Area}} \quad (2)$$

$$\eta_{\text{STF}} = \frac{V_{\text{oc}} \times I_{\text{sc}} \times \text{FF}}{P_{\text{in}} \times \text{Area}} \times \frac{\Delta E \times \xi}{V_{\text{op}}} \times \frac{V_{\text{op}} \times I_{\text{op}}}{V_{\text{oc}} \times I_{\text{sc}} \times \text{FF}} \quad (3)$$

where  $P_{\text{in}}$  is an incident solar power ( $100 \text{ mW}/\text{cm}^2$ ), Area is illuminated electrode area ( $2.10 \text{ cm}^2$ ),  $I_{\text{op}}$  is operating photocurrent (mA),  $\Delta E$  is the thermodynamic potential difference which is 1.33 V for CO generation,  $\xi$  is the F.E. for CO generation (%), and  $V_{\text{op}}$  is the operating potential (V).

Alternatively, STF efficiency can be also calculated by multiplying the efficiency of the PV part with the electrochemical conversion efficiency and their coupling efficiency, as shown in the equation (3); the first term of the product is a power conversion efficiency of CIGS module, the second term is the efficiency of an electrochemical process for CO generation, and the final term is the coupling efficiency between PV parts and electrochemical system. Here, the power conversion efficiency of the CIGS module was 8.58%, as mentioned above, and electrochemical conversion efficiency was 52%. Notably, the coupling efficiency was 94.5%, indicating the efficiency loss by the incorporation of PV and electrochemical cell was not an issue because the operating point of our device successfully maintained close to the maximum power point of the PV module.

From both calculations, the solar to CO conversion efficiency of 4.23% was achieved which means that CO gas was produced in a rate of  $0.4 \mu\text{L}/\text{sec} \cdot \text{cm}^2$ . The operating current density of the device slowly decreased, and thus the solar to CO conversion efficiency decreased to 2.67 % after 5 hr. Finally, in order to confirm whether CO was really originated from  $\text{CO}_2$  reduction,  $^{13}\text{C}$ -isotope test was carried out (see Fig. S4, ESI†). The result clearly verified that the origin of  $^{13}\text{CO}$  was reduced from  $^{13}\text{CO}_2$ .

Our artificial solar-fuel generator demonstrated a 4.23% of solar to fuel conversion efficiency without external bias potential application, which is comparable to photosynthesis of microorganisms and even much higher than most of plants in nature. Moreover, it is a remarkably high value compared to

previous reports so far. For example, Arai *et al.*<sup>33</sup> first reported solar to carbon based fuel conversion efficiency of 0.2% with two semiconductor photoelectrodes in 2013, and later, White *et al.*<sup>34</sup> reported efficiency of 1.8% by using commercial Si solar panel and In-based CO<sub>2</sub> reduction catalyst in 2014.

One of the important advantages of our device is that it is possible to obtain any desired fuel by just changing of the cathode material, which determines the selectivity of CO<sub>2</sub> reduction. For example, by simply replacing nanostructured Au cathode with Pt, only pure hydrogen was obtained with a solar-to-hydrogen conversion efficiency of 4.37% (see Fig. S5 and S6, ESI†).

Our solar-fuel model devices also suggest future research directions and considerations to solve current engineering problems for realization of a higher efficiency. From the STF calculation equation, we could know that the final efficiency (4.23%) of solar-fuel devices is almost half of the power conversion efficiency (8.58%) of the CIGS module, which implies that the developing the performance of the other components besides PV part can almost double the efficiency. We found that the most of efficiency loss was attributed to the electrolysis efficiency (52% in our device) because a decrease in the coupling efficiency was only about 5%. Our device has potential loss of close to 1 V, which can be determined by comparing the operation voltage of 2.33 V with the thermodynamic potential for full reaction of CO generation of 1.33 V. The main sources of the potential loss are overpotentials for oxidation and reduction, potential drop across the membrane, and IR drop due to solution resistance. Based on individual three-electrode tests for the anode (see Fig. 3e) and cathode (see Fig. 4c), we could find that most of the potential loss occurred from the overpotentials, and other sources of potential loss in comparison are not as significant.

Potential loss of approximately 650 mV and 340 mV was attributed to overpotential for OER and CO<sub>2</sub> reduction, respectively. Therefore, to obtain high conversion efficiency, developing catalysts for oxygen evolution reaction is crucial to reduce the overpotential of anode side, especially in neutral pH solution. Although the thermodynamic reduction potential vs. RHE for CO<sub>2</sub> reduction does not depend on pH, hydrogen evolution overcomes CO<sub>2</sub> reduction in acidic solution and CO<sub>2</sub> molecules are hard to exist in a basic solution.<sup>35</sup> Therefore, most of the CO<sub>2</sub> reduction studies have been carried out in a neutral electrolyte as we have used in this study. However, most of the best performing electrocatalysts with low overpotential for water oxidation have been developed in basic solution such as 1 M KOH and their overpotential significantly increases in neutral solution, which is the reason for the large overpotential in our solar-fuel system. This result emphasizes the need in developing optimized oxidation catalysts for solar-fuel devices, and its development can greatly contribute to achieve a higher STF efficiency.

Beyond the catalytic activity issues, the evolved gas bubbles attached on the electrode surface may increase the overpotential (see slow desorption of oxygen bubbles from anode in movie S1, ESI†) which can be resolved by engineering processes such as channel formation on the solar-fuel devices.<sup>36</sup>

As we discussed, decrement of the overpotential for the

oxidation and reduction is important since it can increase the electro-conversion efficiency by reducing potential loss. Or, we can also easily expect that increasing the power conversion efficiency of the PV module will enhance the overall STF efficiency from the equation (3). However, they do not always guarantee the increase of the efficiency for solar-fuel devices because the Faradaic efficiency of CO<sub>2</sub> conversion depends on the applied potential (*i.e.*  $\xi(V_{op})$ ) as shown in Fig. 5b. For the given solar-fuel system, when the overpotential for the water oxidation decreases, the operating point at the intersection of the I-V curve of PV part can be shifted to a higher operating current as we discussed earlier (see Fig. 1c); and if the operating current exceeds a certain level, the Faradaic efficiency for CO<sub>2</sub> reduction on the cathode can rather decrease (see Fig. 5b). To be specific, our model device showed that the Faradaic efficiency for CO<sub>2</sub> reduction decreased when the total current density was larger than ~10 mA (or when the applied bias potential surpassed 2.5 V in the two-electrode system); and consequentially, the final solar-to-fuel conversion efficiency would decrease. This may occur by the mass transfer limitation of CO<sub>2</sub> under high current density or the change of the active sites preferring hydrogen evolution depending on the applied potential. Similarly, if the performance of the PV part increases and enhances the operating potential, the applied potential on cathode side increases which will affect the Faradaic efficiency for CO<sub>2</sub> to CO production. Unlikely solar-water splitting system, the dependence of the Faradaic efficiency on the applied potential at cathode makes it more complicated to realize efficient solar-fuel devices with a target product. To minimize this effect and produce the targeted fuel, it is important to develop CO<sub>2</sub> electrocatalyst with a Faradaic efficiency that is less dependent on the overpotential. But from a different perspective, the dependence can contrarily be advantageous since the product ratio between CO/H<sub>2</sub> can be tuned by changing the photovoltage output from the PV module.

## 4. Conclusions

In brief, by using low cost solution processed CIGS thin film solar cell module technology, low temperature paste coating method of electrocatalytic film for water oxidation, and nanostructured Au cathode for CO<sub>2</sub> reduction; we could achieve a single solar-fuel device operating only by sunlight with solar-to-fuel conversion efficiency of over 4%. This demonstration is just our first step to achieve highly efficient monolithic and standalone solar-fuel device, and even higher efficiency is expected by reducing the overpotential for the water oxidation in the electrolyte. In addition, enhanced performance can be achieved by applying tandem architecture between PV and PC film instead of EC. Vertical series connection of PV instead of a parallel series also allowing us to further reduce photocurrent loss for a high solar-to-fuel conversion efficiency is now under our investigation.

## Acknowledgements

This work was supported by the program of the Korea Institute of Science and Technology (KIST) and partly by the University-Institute cooperation program of the National Research Foundation of Korea Grant funded by the Ministry of Science,

ICT and Future Planning.

## Notes and references

<sup>a</sup> Clean Energy Research Center, Korea Institute of Science and Technology, Hwarangro 14-gil 5, Seongbuk-gu, Seoul 136-791, Republic of Korea. Fax: +82 2 958 5809; Tel: +82 2 958 5853; E-mail: bkmin@kist.re.kr

<sup>b</sup> Korea University of Science and Technology, 176 Gajung-dong, 217 Gajungro Yuseong-gu, Daejeon 305-350, Republic of Korea

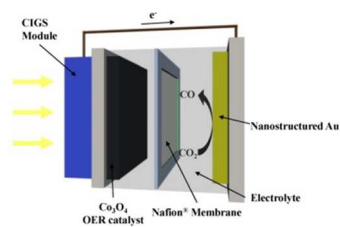
<sup>c</sup> Center for Opto-Electronic Convergence Systems, Korea Institute of Science and Technology, Hwarangro 14-gil 5, Seongbuk-gu, Seoul 136-791, Republic of Korea

<sup>d</sup> Green School, Korea University, Anam-dong, Seongbuk-gu, Seoul, 136-713, Republic of Korea

† Electronic Supplementary Information (ESI) available: See DOI: 10.1039/b000000x/

- 1 J. A. Turner, *Science*, 1999, **285**, 687-689.
- 2 G. Centi, E. A. Quadrelli and S. Perathoner, *Energy Environ. Sci.*, 2013, **6**, 1711-1731.
- 3 N. S. Lewis and D. G. Nocera, *Proc. Natl Acad. Sci. USA*, 2006, **103**, 15729-15735.
- 4 D. Gust, T. A. Moore and A. L. Moore, *Acc. Chem. Res.*, 2009, **42**, 1890-1898.
- 5 A. Kudo, *Int. J. Hydrogen Energy*, 2007, **32**, 2673-2678.
- 6 H. Tong, S. Ouyang, Y. Bi, N. Umezawa, M. Oshikiri and J. Ye, *Adv. Mater.*, 2012, **24**, 229-251.
- 7 S. Bensaid, G. Centi, E. Garrone, S. Perathoner and G. Saracco, *ChemSusChem*, 2012, **5**, 500-521.
- 8 M. R. Hoffmann, S. T. Martin, W. Choi and D. W. Bahnemann, *Chem. Rev.*, 1995, **95**, 69-96.
- 9 S. C. Roy, O. K. Varghese, M. Paulose and C. A. Grimes, *ACS Nano*, 2010, **4**, 1259-1278.
- 10 D. H. Won, C. H. Choi, J. Chung, and S. I. Woo, *Appl. Catal. B*, 2014, **158**, 217-223.
- 11 X.-G. Zhu, S. P. Long and D. R. Ort, *Annu. Rev. Plant Biol.*, 2010, **61**, 235-261.
- 12 R. E. Blankenship, D. M. Tiede, J. Barber, G. W. Brudvig, G. Fleming, M. Ghirardi, M. R. Gunner, W. Junge, D. M. Kramer, A. Melis, T. A. Moore, C. C. Moser, D. G. Nocera, A. J. Nozik, D. R. Ort, W. W. Parson, R. C. Prince and R. T. Sayre, *Science*, 2011, **332**, 805-809.
- 13 D. Walker, *J. Appl. Phycol.*, 2009, **21**, 509-517.
- 14 A. Fujishima and K. Honda, *Nature*, 1972, **238**, 37-38.
- 15 S. Y. Reece, J. A. Hamel, K. Sung, T. D. Jarvi, A. J. Esswein, J. J. H. Pijpers and D. G. Nocera, *Science*, 2011, **334**, 645-648.
- 16 O. Khaselev and J. A. Turner, *Science*, 1998, **280**, 425-427.
- 17 Y. Surendranath, D. K. Bediako and D. G. Nocera, *Proc. Natl Acad. Sci. USA*, 2012, **109**, 15617-15621.
- 18 S. Licht, B. Wang, S. Mukerji, T. Soga, M. Umeno and H. Tributsch, *J. Phys. Chem. B*, 2000, **104**, 8920-8924.
- 19 A. J. Nozik, *Appl. Phys. Lett.*, 1977, **30**, 567-569.
- 20 L. J. Minggu, W. R. Wan Daud and M. B. Kassim, *Int. J. Hydrogen Energy*, 2010, **35**, 5233-5244.
- 21 T. J. Jacobsson, V. Fjallstrom, M. Sahlberg, M. Edoff and T. Edvinsson, *Energy Environ. Sci.*, 2013, **6**, 3676-3683.
- 22 H. Doscher, J. F. Geisz, T. G. Deutsch and J. A. Turner, *Energy Environ. Sci.*, 2014, **7**, 2951-2956.
- 23 S. E. Habas, H. A. S. Platt, M. F. A. M. van Hest and D. S. Ginley, *Chem. Rev.*, 2010, **110**, 6571-6594.
- 24 Y. Chen, C. W. Li and M. W. Kanan, *J. Am. Chem. Soc.*, 2012, **134**, 19969-19972.
- 25 S. J. Park, J. W. Cho, J. K. Lee, K. Shin, J.-H. Kim and B. K. Min, *Prog. Photovolt: Res. Appl.*, 2014, **22**, 122-128.
- 26 S. J. Park, Y. Cho, S. H. Moon, J. E. Kim, D.-K. Lee, J. Gwak, J. Kim, D.-W. Kim and B. K. Min, *J. Phys. D: Appl. Phys.*, 2014, **47**, 135105.
- 27 D. G. H. Hetterscheid, J. I. van der Vlugt, B. de Bruin and J. N. H. Reek, *Angew. Chem. Int. Ed.*, 2009, **48**, 8178-8181.
- 28 H. S. Jeon, W. Park, J. Kim, H. Kim, W. Kim and B. K. Min, *Int. J. Hydrogen Energy*, 2011, **36**, 1924-1929.
- 29 H. S. Jeon, A. Nugroho, J. Kim, H. Kim and B. K. Min, *Int. J. Hydrogen Energy*, 2011, **36**, 10587-10592.
- 30 T. Hatsukade, K. P. Kuhl, E. R. Cave, D. N. Abram and T. F. Jaramillo, *Phys. Chem. Chem. Phys.*, 2014, **16**, 13814-13819.
- 31 Z. Chen, T. F. Jaramillo, T. G. Deutsch, A. Kleiman-Shwarsstein, A. J. Forman, N. Gaillard, R. Garland, K. Takanebe, C. Heske, M. Sunkara, E. W. McFarland, K. Domen, E. L. Miller, J. A. Turner and H. N. Dinh, *J. Mater. Res.*, 2010, **25**, 3-16.
- 32 M. T. Winkler, C. R. Cox, D. G. Nocera and T. Buonassisi, *Proc. Natl Acad. Sci. USA*, 2013, **110**, E1076-E1082.
- 33 T. Arai, S. Sato, T. Kajino and T. Morikawa, *Energy Environ. Sci.*, 2013, **6**, 1274-1282.
- 34 J. L. White, J. T. Herb, J. J. Kaczur, P. W. Majsztzik and A. B. Bocarsly, *J. CO<sub>2</sub> Util.*, 2014, **7**, 1-5.
- 35 Y. Hori, in *Modern Aspects of Electrochemistry*, eds. C. Vayenas, R. White and M. Gamboa-Aldeco, Springer New York, 2008, vol. 42, ch. 3, pp. 89-189.
- 36 M. J. Cheah, I. G. Kevrekidis and J. B. Benziger, *Langmuir*, 2013, **29**, 9918-9934.

## A table of contents (TOC)



5

A standalone solar-fuel device producing CO from CO<sub>2</sub> is developed via integration with a solution processed CIGS module and electrocatalysts, achieving a solar-to-fuel conversion efficiency over 4 %.

10

15